Available online at www.sciencedirect.com
ScienceDirect
Journal of Solid State Chemistry 181 (2008) 976–982
JOURNAL OF SOLID STATE CHEMISTRY
www.elsevier.com/locate/jssc

Topotactic insertion of lithium in the layered structure $Li_4VO(PO_4)_2$: The tunnel structure $Li_5VO(PO_4)_2$

M. Satya Kishore[a], V. Pralong[a,*], V. Caignaert[a], S. Malo[a], S. Hebert[a], U.V. Varadaraju[b], B. Raveau[a]

[a]*Laboratoire de Cristallographie et Sciences des Matériaux, ENSICAEN, Université de Caen, CNRS, 6 Bd Maréchal Juin, F-14050 Caen 4, France*
[b]*Materials Science Research Centre, Indian Institute of Technology Madras, Chennai 6000036, India*

Received 23 October 2007; received in revised form 4 January 2008; accepted 18 January 2008
Available online 12 February 2008

Abstract

A new V(III) lithium phosphate $Li_5VO(PO_4)_2$ has been synthesized by electrochemical insertion of lithium into $Li_4VO(PO_4)_2$. This phase, which crystallizes in the space group *I*4/*mcm*, exhibits a tunnel structure closely related to the layered structure of $Li_4VO(PO_4)_2$ and to the tunnel structure of $VO(H_2PO_4)_2$. The topotactic reactions that take place during lithium exchange and intercalation, starting from $VO(H_2PO_4)_2$ and going to the final phase $Li_5VO(PO_4)_2$ are explained on the basis of the flexible coordinations of V^{4+} and V^{3+} species. The electrochemical and magnetic properties of this new phase are also presented and explained on the basis of the structure dimensionality.

Keywords: $Li_5VO(PO_4)_2$; Intercalation; Li-ion battery; TEM; Vanadium phosphate

1. Introduction

Vanadium-based phosphates are of considerable interest because of their versatile chemical/physical properties such as ion exchange, redox chemistry, intercalation, catalysis and magnetic properties [1,2]. In particular, vanadium exhibits a flexible coordination and various oxidation states (III, IV, V) in phosphates, which make vanadium-based phosphates attractive as electrode materials for Li-ion batteries. Good reversibility of lithium was demonstrated for V^{3+}/V^{4+} redox couple in vanadium containing phosphates such as $Li_3V_2(PO_4)_3$ [3–5], $LiVP_2O_7$ [6,7], $LiVPO_4F$ [8], $Li_5V(PO_4)_2F_2$ [9] and for V^{4+}/V^{5+} in $LiVOPO_4$ [10,11], $VOPO_4$ [12–14].

We have recently reported the synthesis and structure of a new vanadyl(IV) phosphate, $Li_4VO(PO_4)_2$ [15]. The latter has a layered structure involving $[V_2P_4O_{18}]_\infty$ layers built up of successive chains of VO_6 octahedra and VO_5 pyramids interconnected by isolated PO_4 tetrahedra [16]. The Li^+ ions present in between these layers are reversibly extracted/inserted, in agreement with the presence of the redox couple V^{4+}/V^{5+}. This material exhibits a reversible capacity of ~60 mAh/g at 4.1 V vs. Li/Li^+ [15]. The presence of tetravalent vanadium in this phosphate suggests the possibility of insertion of one additional lithium into the structure by reducing V^{4+} into V^{3+}. In this paper, we have studied the electrochemical lithium insertion into $Li_4VO(PO_4)_2$. We have synthesized in this way a new V(III) diphosphate $Li_5VO(PO_4)_2$, whose structure is closely related to that of $Li_4VO(PO_4)_2$, but differs from the latter by its three-dimensional character. The topotactic nature of the reaction involving the lithium vanadyl phosphate and the protonic phosphate $VO(H_2PO_4)_2$ is also discussed.

2. Experimental

The synthesis of $Li_4VO(PO_4)_2$ was performed by ion exchange method starting from $VO(H_2PO_4)_2$. Lithium intercalation into this phase has been carried out electrochemically using Swagelok type cells. The cells were assembled in an argon filled glove box, with lithium metal

*Corresponding author. Fax: +33 2 31 95 16 00.
E-mail address: valerie.pralong@ensicaen.fr (V. Pralong).

0022-4596/$ - see front matter © 2008 Published by Elsevier Inc.
doi:10.1016/j.jssc.2008.01.044

as the negative electrode and a borosilicate glass fiber sheet as separator and saturated with 1 M $LiPF_6$ in 1:1 ethylene carbonate (EC): dimethyl carbonate (DMC) (LP30, Merck) as the electrolyte. The composite positive electrode was prepared by mixing 80 wt% active material with 20 wt% acetylene black. The electrochemical reactivity was monitored with a VMP II potentiostat/galvanostat (Biologic SA, Claix, France) at room temperature (20 °C).

The samples were characterized by powder X-ray diffraction (XRD). XRD patterns were collected on Philips X'pert diffractometer with Bragg–Brentano geometry (Cu$K\alpha$ radiation). The *ex situ* XRD patterns of the electrodes were registered under vacuum using a chamber attached to the XRD instrument.

The electron diffraction (ED) study was carried out on a JEOL 200CX electron microscope fitted with an eucentric goniometer ($\pm 60^\circ$) equipped with an EDS (Energy Dispersive Spectroscopy) analyser at room temperature. For the transmission electron microscopy study, the samples were crushed in *n*-butanol and deposited on a holey carbon membrane supported by a copper grid.

Magnetic measurements were carried out in the temperature range between 5 and 400 K with a SQUID Magnetometer, in a field of 0.3 T.

3. Results and discussion

3.1. Synthesis of $Li_5VO(PO_4)_2$

The electrochemical synthesis of $Li_5VO(PO_4)_2$ was performed at a $C/50$ rate. Starting from $Li_4VO(PO_4)_2$, the cell was discharged to 1.3 V and one can observe a plateau at 1.67 V (Fig. 1). One Li (94 mAh/g) is inserted by discharging the cell to 1.3 V that corresponds to the complete reduction of V^{4+} to V^{3+}. In the literature, in phosphate hosts, the V^{4+}/V^{3+} redox couple is observed at 3.5–4.0 V [3–7]. Two hypotheses could be suggested in order to explain such low voltage (1.67 V instead of 3.5 V): either a structural change or a decomposition of the compound. In both cases the signature would be a well-defined plateau associated with a sharp peak (<200 mV) on the derivative curve (inset, Fig. 1) and in addition, these transformations needs energy. In order to understand the origin of this low potential, we have registered *ex situ* XRD patterns (Fig. 2). The XRD patterns of the two phases, $Li_4VO(PO_4)_2$ (Fig. 2a) and $Li_5VO(PO_4)_2$ (Fig. 2c) show sharp peaks indicative of a good cristallinity. The XRD pattern registered at the middle of the plateau shows the reflections ascribed to the two end members $Li_4VO(PO_4)_2$ and $Li_5VO(PO_4)_2$ (Fig. 2b). New reflections are observed for $Li_5VO(PO_4)_2$, requiring a complete structure determination.

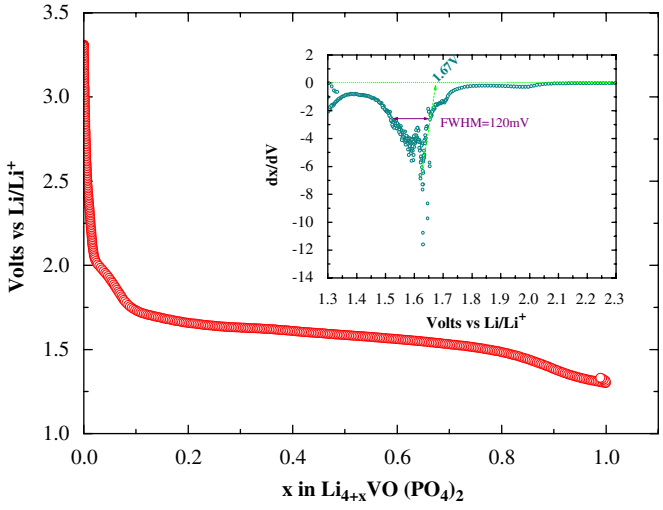

Fig. 1. Voltage vs. composition curve for the first discharge for $Li_4VO(PO_4)_2$ at $C/50$ rate to 1.3 V; inset: corresponding derivative curve.

3.2. Structure of $Li_5VO(PO_4)_2$: relationship with $Li_4VO(PO_4)_2$ and $VO(H_2PO_4)_2$

The crystal structure of $Li_5VO(PO_4)_2$ is solved by combining the powder XRD data and electron diffraction study. The initial pattern matching result of X-ray powder pattern of $Li_5VO(PO_4)_2$ shows that it can be indexed on a tetragonal cell $a = 9.185(3)$ Å, $c = 7.967(3)$ Å. It is worth mentioning here that the parent phase, $Li_4VO(PO_4)_2$ crystallizes in $P4/n$ space group with $a = 8.8204(1)$ Å, $c = 8.7614(2)$ Å. Thus, with lithium insertion one observes an increase of the '*a*' lattice parameter and a decrease of the '*c*' parameter, whereas the cell volume decreases from 681.64(1) to 672.26(3) Å^3. The Rietveld refinement of $Li_5VO(PO_4)_2$ with $P4/n$ space group did not allow a *R*-factor lower than 0.1 to be obtained. Thus, a possible change in the symmetry was considered and hence an electron diffraction study was carried out.

The ED patterns of $Li_5VO(PO_4)_2$ recorded along [0 0 1], [1 0 0] and [1 $\bar{1}$ 0] are displayed as examples in Fig. 3. They

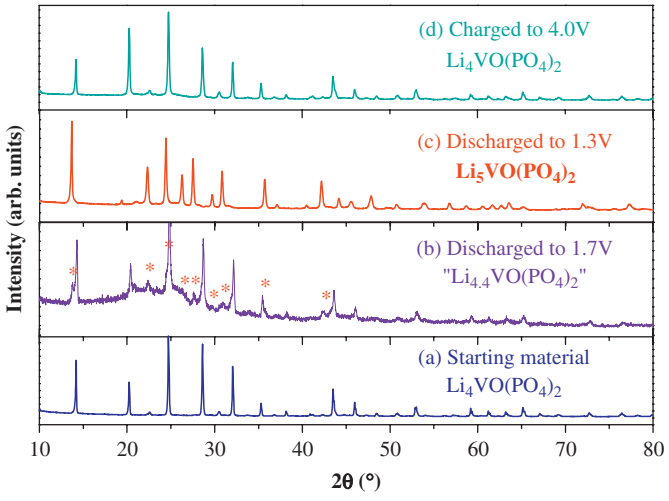

Fig. 2. *Ex situ* XRD patterns of (a) parent phase, $Li_4VO(PO_4)_2$; (b) after 0.4 lithium insertion, showing the biphasic process (star indicates the reflections of $Li_5VO(PO_4)$); (c) after one lithium insertion, $Li_5VO(PO_4)_2$ and (d) after extraction of one lithium, $Li_4VO(PO_4)_2$.

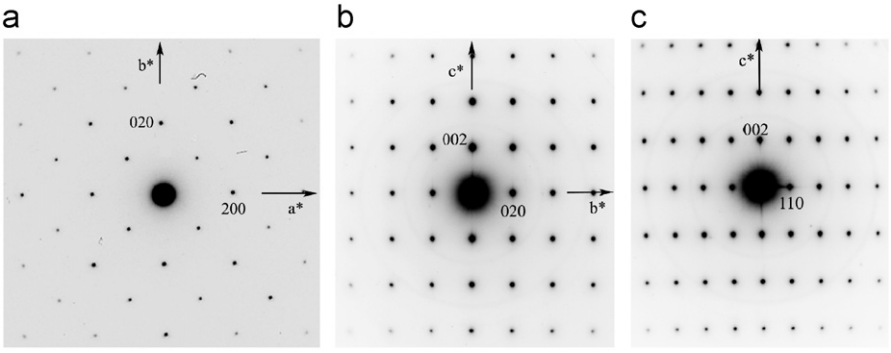

Fig. 3. Electron diffraction patterns recorded on $Li_5VO(PO_4)_2$ along (a) [0 0 1], (b) [1 0 0] and (c) [1 $\bar{1}$ 0] directions.

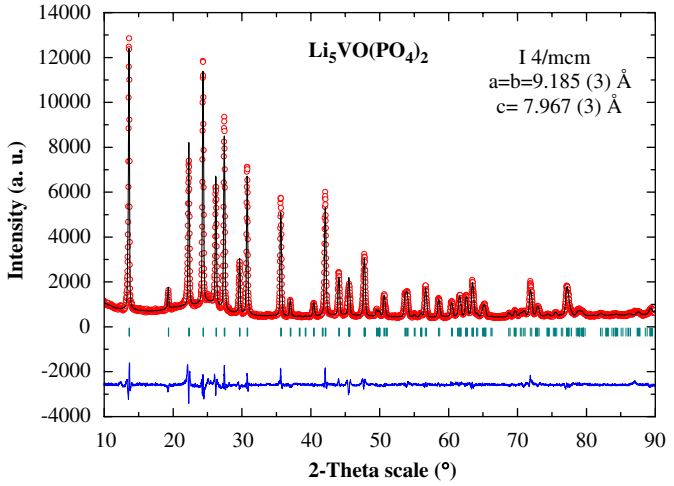

Fig. 4. Rietveld refinement plot of X-ray diffraction data for $Li_5VO(PO_4)_2$. Observed, calculated, and difference profiles are plotted on the same scale. The Bragg peaks are indicated by tick marks.

evidence a tetragonal cell with $a \approx 9.2$ Å and $c \approx 8$ Å. The reciprocal space was reconstructed by tilting around the different axes. The conditions limiting the reflections *hkl*: $h+k+l=2n$ and *h*0*l*: $l=2n$ are consistent with the space groups $I4/mcm$, $I4cm$ and $I\bar{4}cm$. The Rietveld refinement was performed with the most symmetrical space group, $I4/mcm$ and the corresponding fit is shown in Fig. 4. The structure solution was searched manually and in fact, the lithium positions were detected from the difference Fourier map of the XRD data. The atomic positions of V and P were first refined, followed by the refinement of Li and O atomic positions. The refinement of the isothermal parameters led to the convergence of the agreement factors to $\chi^2 = 0.052$, R_f-factor = 0.051, Bragg *R*-factor = 0.059. Refinement of the occupancy factors of the V and O sites showed that they are fully occupied. The final structural parameters and the refined atomic positions with the thermal parameters are given in Tables 1 and 2, respectively.

The cell parameters of $Li_5VO(PO_4)_2$, close to those of $VO(H_2PO_4)_2$ and $Li_4VO(PO_4)_2$, strongly support the fact that the intercalation/exchange reactions that take place from $VO(H_2PO_4)_2$ are topotactic. The projection of the

Table 1
Crystallographic data for $Li_5VO(PO_4)_2$

Formula	$Li_5VO(PO_4)_2$
Fw (g/mol)	291.94
Space group	$I4/mcm$ (140)
a, *b* (Å)	9.185(3)
c (Å)	7.967(3)
V (Å^3)	672.2(3)
Z	4
ρ_{calc} (g/cm^3)	2.88117
χ^2 (%)	5.28
R_f-factor (%)	5.16
Bragg *R*-facto (%)	5.93

Table 2
Fractional atomic coordinates and isotropic thermal factors for $Li_5VO(PO_4)_2$

Atom	Wyck.	*x*/*a*	*y*/*b*	*z*/*c*	*U* (Å^2)
V	4*c*	0	0	0	0.0692(8)
P	8*h*	0.29444(19)	0.79444(19)	0	0.1536(7)
O1	4*a*	0	0	1/4	0.037(3)
O2	16*l*	0.36342(2)	0.86342(2)	0.15848(4)	0.0341(15)
O3	16*k*	0.18033(3)	0.12512(3)	0	0.0263(15)
Li1	4*b*	0	1/2	1/4	0.026(4)
Li2	16*j*	0	0.2249(11)	1/4	0.026(4)

three structures along *c* (Fig. 5) and along *a* (Fig. 6) show the great similarity. Both phosphates $VO(H_2PO_4)_2$ (Figs. 5a and 6a) and $Li_5VO(PO_4)_2$ (Figs. 5c and 6c) exhibit a three-dimensional framework of corner sharing VO_6 octahedra and PO_4 tetrahedra forming similar tunnels running along *c*. One indeed observes $[VO_3]_\infty$ chains of corner sharing octahedra running along *c* and interconnected through single PO_4 tetrahedra. Nevertheless, these two compounds differ from each other by the relative positions of the H and Li atoms in the tunnels, involving different space groups, $P4/nnc$ and $I4/mcm$, respectively. The phosphate $Li_4VO(PO_4)_2$, in spite of its great structural similarity along *c* (Fig. 5b), differs fundamentally from the two other phases, as shown by the view of its structure along *a* (Fig. 6b): the $[VO_3]_\infty$ octahedral rows are interrupted every two polyhedra, forming "V_2O_{10}" dimers

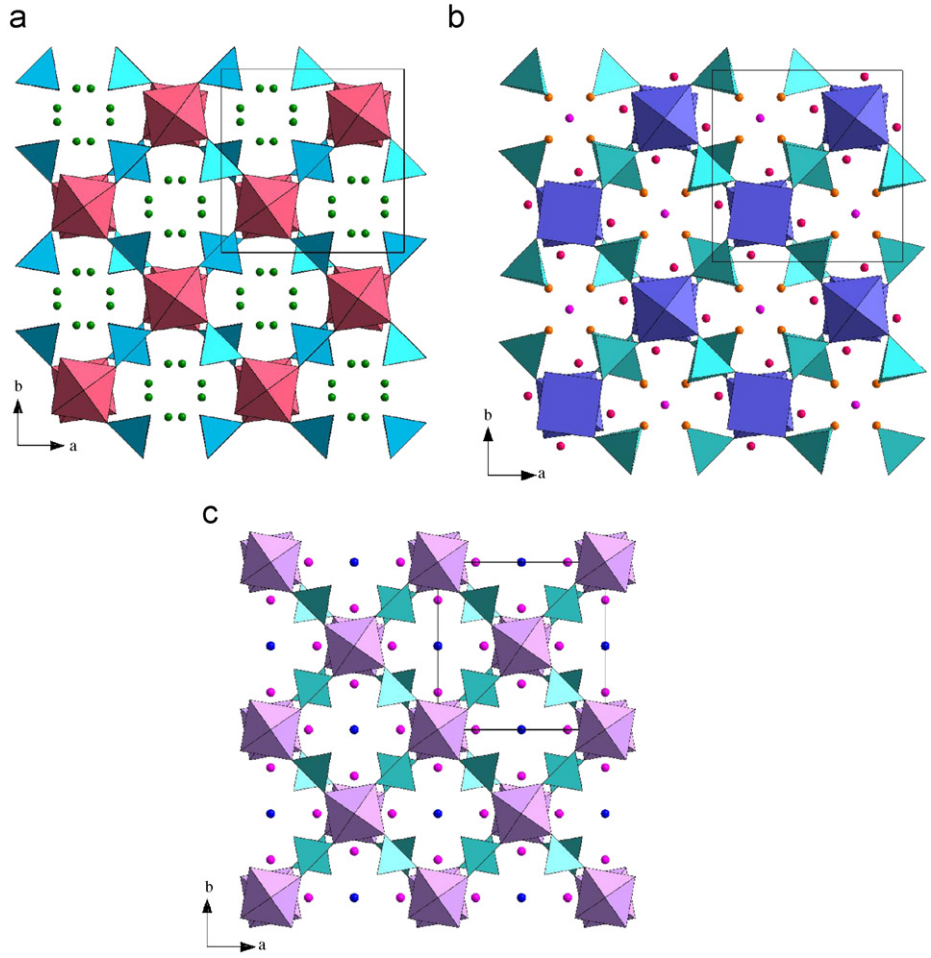

Fig. 5. Structure of $VO(H_2PO_4)_2$ (a), $Li_4VO(PO_4)_2$ (b), $Li_5VO(PO_4)_2$ (c) viewed along the *c* direction.

built up of one VO_6 octahedron and one VO_5 pyramid. Thus, $Li_4VO(PO_4)_2$ exhibits a layered structure with a different space group, $P4/n$. From this structural analysis, it appears that the topotactic reactions that take place during these syntheses may appear at first sight rather strange, since they imply the intermediate formation of a layered structure between two very closely related tunnel structures according to the sequence:

$$\underset{V^{4+}\ 3D}{VO(H_2PO_4)_2} \xrightarrow{LiBr:hexanol} \underset{V^{4+}\ 2D}{Li_4VO(PO_4)_2} \xrightarrow{Electrochem.} \underset{V^{3+}\ 3D}{Li_5VO(PO_4)_2}.$$

Another interesting feature deals with the fact that the cell volume of $Li_5VO(PO_4)_2$ is smaller than that of $Li_4VO(PO_4)_2$ in spite of the increase of the size of the vanadium cation resulting from the reduction of V(IV) into V(III). The comparison of the V–O distances for the three compounds (Table 3) and of the geometry of the VO_6 octahedra and VO_5 pyramids allows to shed light on this issue. The average V–O distances in $VO(H_2PO_4)_2$ and $Li_4VO(PO_4)_2$, ranging from 1.92 to 1.977 Å are smaller than that of $Li_5VO(PO_4)_2$ (2.00 Å), in agreement with the smaller size of V^{4+} species compared to V^{3+}. More importantly, one observes that the apical V–O distances of the VO_6 octahedra of $VO(H_2PO_4)_2$ and of $Li_4VO(PO_4)_2$ are very dissymmetric, as often observed for V^{4+} oxides. One indeed observes apical bonds of 1.597 and 2.385 Å for the former, and of 1.77 and 2.06 Å for the second one. In contrast, the VO_6 octahedra of $Li_5VO(PO_4)_2$ are practically regular, with V–O distances ranging from 1.99 to 2.01 Å, as usually observed for V^{3+}.

The bond valence sum calculation [17] of the new structure (Table 4) supports also strongly the trivalent character of vanadium, leading to a valence of 2.93. In those structures, the geometry of the PO_4 tetrahedra does not vary significantly ranging from 1.49 to 1.57 Å. In the same way, lithium in the Li1 site adopts a perfect tetrahedral coordination in both structures, with Li–O distances close to 1.92 Å. In contrast, one observes a large distortion of the other Li polyhedra. In $Li_5VO(PO_4)_2$ the second lithium (Li2) exhibits a strongly distorted pyramidal coordination with Li–O distances ranging from 1.93 to 2.33 Å, whereas $Li_4VO(PO_4)_2$ exhibits two other Li sites, a pyramidal one with Li–O distances ranging from 1.963 to 2.223 Å, and a strongly distorted tetrahedral one with distances ranging from 1.88 to 2.264 Å.

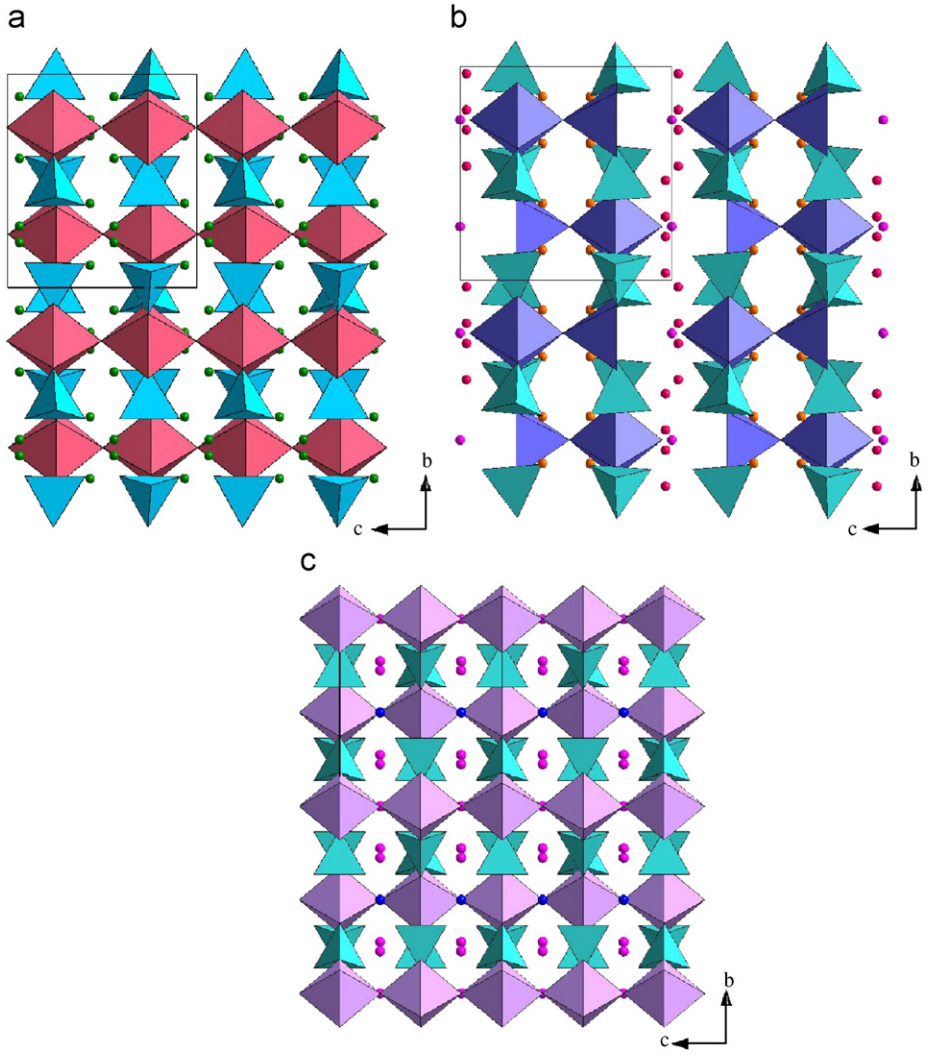

Fig. 6. Structure of $VO(H_2PO_4)_2$ (a), $Li_4VO(PO_4)_2$ (b), $Li_5VO(PO_4)_2$ (c) viewed along the *a* direction.

Table 3
Comparison of the V–O distances (Å) for the three compounds

	$Li_5VO(PO_4)_2$	$Li_4VO(PO_4)_2$	$VO(H_2PO_4)_2$
V–O	1.991 × 2 (O1)	1.789 × 1 (O5)	1.597 × 1 (O3)
V–O	2.016 × 4 (O3)	1.954 × 4 (O9)	1.978 × 4 (O1)
V–O			2.385 × 1 (O3)

Table 4
The bond valence sum calculation of the new structure $Li_5VO(PO_4)_2$

	Valence
V	2.936
P	4.668
Li1	1.18
Li2	0.96
O1	2.274
O2	2.115
O3	2.052

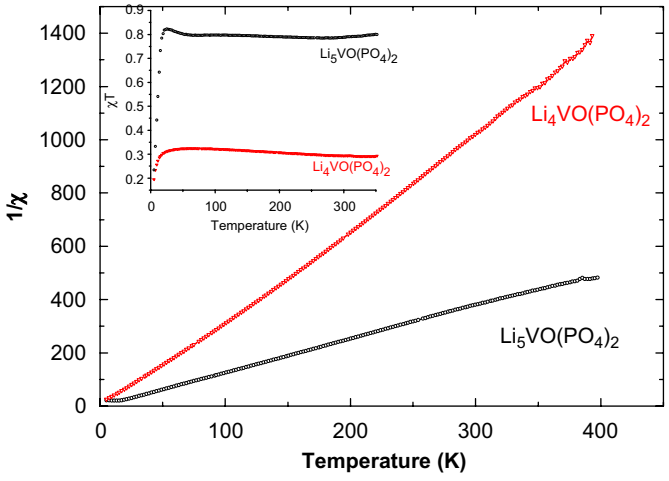

Fig. 7. Reciprocal magnetic susceptibility of $Li_4VO(PO_4)_2$ and $Li_5VO(PO_4)_2$ as a function of temperature. Inset: χT vs. T for $Li_4VO(PO_4)_2$ and $Li_5VO(PO_4)_2$.

From these results, the topotactic reactions in these materials can be explained in the following way. As lithium is exchanged for protons in $VO(H_2PO_4)_2$, it expands dramatically the *c* parameter of the tetragonal cell, so that one apical oxygen out of two is strongly displaced along *c*, leading to the formation of VO_5 pyramids in $Li_4VO(PO_4)_2$. In contrast, when lithium is electrochemically intercalated in the latter structure, the reduction of V^{4+} into V^{3+} requires the formation of more symmetric bonds, i.e. regular octahedra and consequently the *c* axis is decreased, whereas the *a* parameter is increased. The slightly smaller volume of $Li_5VO(PO_4)_2$ with respect to $Li_4VO(PO_4)_2$ is then explained by a change of distribution and coordination of the lithium cations in the structure, which can be considered as electro-attractive species with respect to the surrounding oxygen atoms.

3.3. Magnetic properties

The reciprocal magnetic susceptibility curves $\chi^{-1}(T)$ vs. temperature of $Li_4VO(PO_4)_2$ and $Li_5VO(PO_4)_2$ (Fig. 7) show that above 20 K, both compounds follow the Curie–Weiss law. The effective magnetic moment obtained from these data, of 1.74 μ_B/f.u. for the first one and of 2.61 μ_B/f.u. for the second one are in perfect agreement with the calculated values for V^{4+} (1.73 μ_B) and V^{3+} (2.83 μ_B) species, respectively. These results corroborate the above structural and electrochemical results concerning the reduction of V^{4+} into V^{3+} during the lithium insertion. Below 20 K, the $c(T)$ curves (inset Fig. 7) show a sharp drop of the magnetic susceptibility indicating the presence of weak antiferromagnetic interactions. This kind of weak antiferromagnetic interactions are

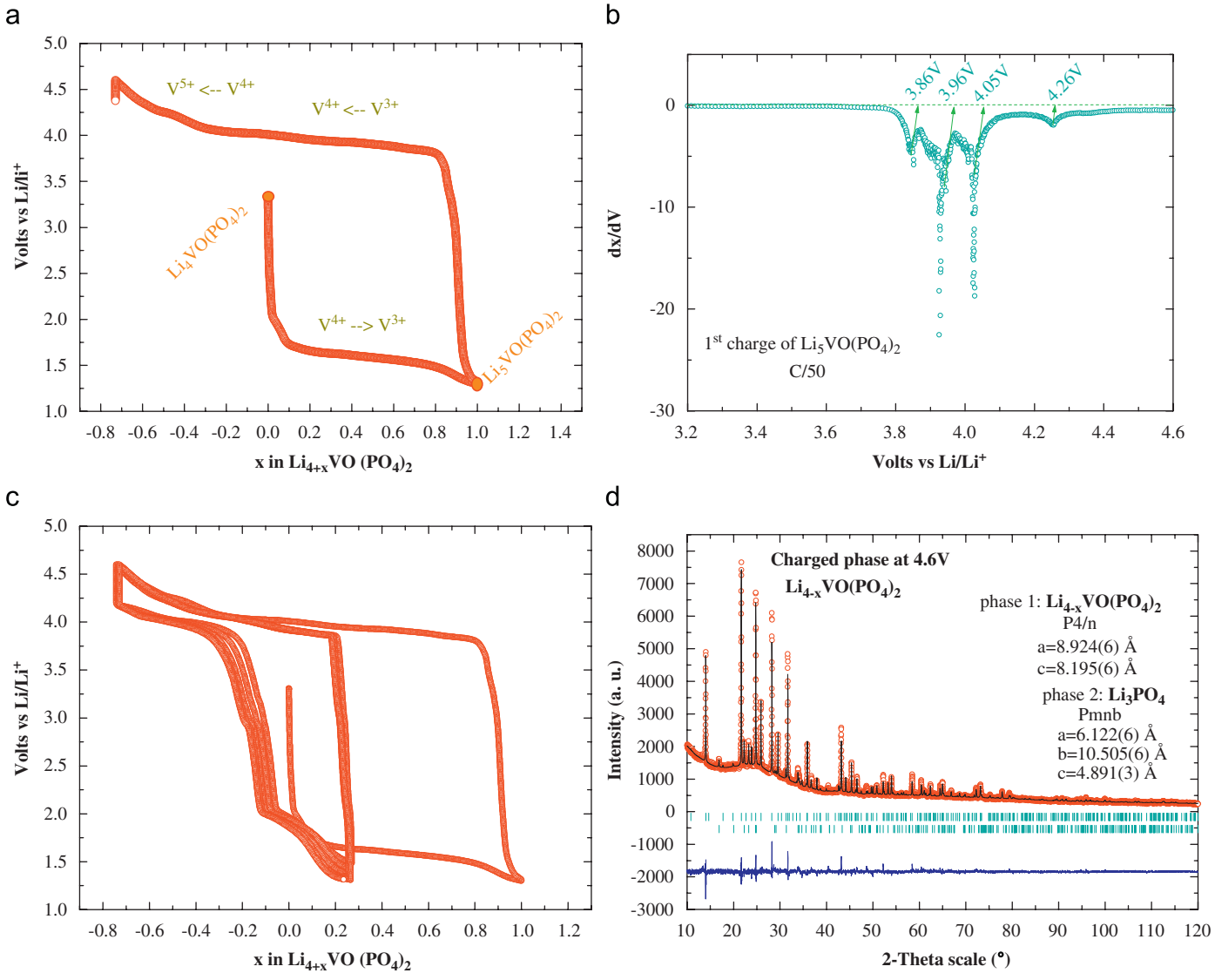

Fig. 8. (a) First discharge and charge of $Li_4VO(PO_4)_2$ at *C*/50 rate to 1.3 V; (b) derivative curve of the first charge; (c) cycling behaviour in the potential window 1.3–4.6 V; (d) Rietveld refinement plot of X-ray diffraction data for $Li_{4-x}VO(PO_4)_2$ at 4.6 V, showing the partial decomposition of the compound into Li_3PO_4.

known in other V phosphates such as β-$LiVOPO_4$ [18], $AV_2O(PO_4)_2$ ($A = Cd$, Ca, Sr) [19], $AVO(PO_4)_2 \cdot 4H_2O$ ($A = Pb$, Ba) [20].

3.4. Cycling behaviour of $Li_5VO(PO_4)_2$

The initial charge profile, starting from $Li_5VO(PO_4)_2$ at 1.3 V, shows that lithium is extracted above 3.5 V (Fig. 8a). By charging the cell to 4.6 V, 1.8 lithium ions are extracted. The extraction of a large amount of lithium together with the charge potential, clearly suggest that the V(III) in $Li_5VO(PO_4)_2$ is oxidized first to V(IV) and finally to V(V). Interestingly, we can observe on the derivative curve (Fig. 8b) four peaks at 3.86, 3.96, 4.05 and 4.26 V, respectively. The XRD pattern taken after the extraction of 1.0Li, i.e. 4 V, is shown in Fig. 2d. In spite of changes in the relative intensities due to the preferential orientation of the sample, the XRD pattern is similar to that of the parent phase $Li_4VO(PO_4)_2$. This suggests that the deintercalation into the parent structure appears through a biphasic process. Thus, we can ascribe the first two signatures on the derivative curve to the oxidation of V(III) into V(IV). These two peaks, clearly observable (3.86 and 3.96 V) confirm the existence of two cristallographic sites Li1 and Li2 in the structure of $Li_5VO(PO_4)_2$. At higher potential two peaks at 4.05 and 4.26 V are observed, which correspond to the oxidation of V(IV) into V(V). Nevertheless, at the end of the charge, the limit member $Li_3VO(PO_4)_2$ containing only V(V) is not stable. A decomposition reaction takes place with the formation of Li_3PO_4 as a secondary phase (Fig. 8d).

On further cycling, 0.5Li insertion is observed at high voltage and 0.5Li is intercalated at lower voltage region (Fig. 8c). Curiously, no intercalation is observed when cycling was carried out in the potential window 1.3–4 V. In fact, the large polarization of the potential between the charge and discharge may be due to the structural transition from 2D for $Li_4VO(PO_4)_2$ to 3D for $Li_5VO(PO_4)_2$. This difference in dimensionality between the two structures hinders a good reversibility in cycling.

4. Conclusion

These results, together with those previously obtained for the protonic phosphate $VO(H_2PO_4)_2$ [15,16], show the extraordinary flexibility of the "framework" $VO(PO_4)_2$, which can accommodate either a 3D or a 2D configuration, through lithium exchange or intercalation. Such topotactic reactions are possible due to the great flexibility of V^{4+} coordination, intermediate between pyramidal and octahedral and to its ability to be reduced into V^{3+}. The ability of lithium to accommodate various distorted coordinations is also an important factor which favours such reactions. From the view point of electrochemistry, a good reversibility in cycling cannot be obtained between $Li_4VO(PO_4)_2$ and $Li_5VO(PO_4)_2$. These results are of great interest, since they open the route of the exploration of protonic vanadophosphates in view of lithium intercalation.

Acknowledgments

Financial support from IFCPAR (Indo-French Centre for the Promotion of Advanced Research/Centre Franco-Indien Pour la Promotion de la Recherche Avancee) and LAFICS program is gratefully acknowledged.

References

[1] S. Boudin, A. Guesdon, A. Leclaire, M.-M. Borel, Int. J. Inorg. Mater. 2 (2000) 561.
[2] J. Kalousová, J. Votinskỳ, L. Beneš, K. Melánová, V. Zima, Collect. Czech. Chem. Commun. 63 (1998) 1.
[3] J. Gaubicher, C. Wurm, G. Goward, C. Masquelier, L. Nazar, Chem. Mater. 12 (2000) 3240.
[4] M.Y. Saidi, J. Barker, H. Huang, J.L. Swoyer, G. Adamson, Electrochem. Solid State Lett. 5 (2002) A149.
[5] H. Huang, S.-C. Yin, T. Kerr, N. Taylor, L.F. Nazar, Adv. Mater. 14 (2002) 1525.
[6] C. Wurm, M. Morcrette, G. Rousse, L. Dupont, C. Masquelier, Chem. Mater. 14 (2002) 2701.
[7] Y. Uebou, S. Okada, M. Egashira, J.-I. Yamaki, Solid State Ionics 148 (2002) 323.
[8] J. Barker, M.Y. Saide, J.L. Swoyer, J. Electrochem. Soc. 150 (2003) A1394.
[9] S.-C. Yin, P. Subramanya Herle, A. Huggins, N.J. Taylor, Y. Makimura, L.F. Nazar, Chem. Mater. 18 (2006) 1745.
[10] J. Barker, M.Y. Saidi, J.L. Swoyer, J. Electrochem. Soc. 151 (2004) A796.
[11] J. Gaubicher, T. Le Mercier, Y. Chabre, J. Angenault, M. Quarton, J. Electrochem. Soc. 146 (1999) 4375.
[12] N. Dupré, J. Gaubicher, T. Le Mercier, G. Wallez, J. Angenault, M. Quarton, Solid State Ionics 140 (2001) 209.
[13] B.M. Azmi, T. Ishihara, H. Nishiguchi, Y. Takita, J. Power Sources 119–121 (2003) 273.
[14] Y. Song, P.Y. Zavalii, M.S. Whittingham, J. Electrochem. Soc. 152 (2005) A721.
[15] M. Satya Kishore, V. Pralong, V. Caignaert, U.V. Varadaraju, B. Raveau, Electrochem. Commun. 8 (2006) 1558.
[16] V. Caignaert, M. Satya kishore, V. Pralong, B. Raveau, N. Creon, H. Fjellvåg, J. Solid State Chem. 180 (9) (2007) 2437–2442.
[17] Valist.exe, valence and bonds distance calculation program from Andrew Wills. 〈ftp://ftp.ill.fr/pub/dif/valist〉.
[18] K.H. Lii, C.H. Li, C.Y. Cheng, S.L. Wang, J. Solid State Chem. 95 (1991) 352.
[19] S. Boudin, A. Grandin, Ph. Labbé, J. Provost, B. Raveau, J. Solid State Chem. 127 (1996) 325.
[20] M. Roca, P. Amorós, J. Cano, M. Dolores Marcos, J. Alamo, A. Beltrán-Porter, D. Beltrán-Porter, Inorg. Chem. 37 (1998) 3167.